Improved Angular Resolution of Neuronal Fiber Segmentation in Diffusion Magnetic Resonance Imaging

Staunton G. H. Golding[1], Adam W. Anderson PhD[1,2]

[1]Department of Biomedical Engineering, Vanderbilt University [2]Vanderbilt University Institute of Imaging Sciences

Introduction

Diffusion of water in the white matter of the brain is constrained by axonal and other cellular membranes; hence, diffusion weighted magnetic resonance imaging (DMRI) provides a way to estimate the orientation and distribution of neuronal fiber bundles in the white matter of the brain, modeled as fiber orientation distribution functions (FODFs). Each discrete peak of the FODF corresponds to a uniquely oriented fiber population. Current methods to elucidate fiber bundle orientations from FODFs extract only one fiber bundle element (fixel) per FODF lobe. These approaches offer an angular resolution of ~45° between fixels (1).

It is estimated that approximately 90% of white matter voxels contain more than one fiber element (1), but with their angular resolution, lobe-based fixel segmentation methods can identify multiple fixels in only ~45% of voxels. This implies the true complexity of fiber angular distributions is underestimated. This loss in geometric complexity limits the accuracy of downstream analyses, such as fiber tract reconstruction and brain connectomics. Most attempts at improving angular resolution focus on a robust signal to FODF conversion (1, 2, 3). We propose an alternate, novel super-resolution approach for the detection of unresolved fixels. Our method allows for the identification of more than one fixel per FODF lobe and is based on the following observation: FODFs of parallel fiber populations demonstrate cylindrical symmetry about the fiber axis (1), so cylindrical asymmetry in FODF lobes suggests the presence of non-parallel fiber populations.

Method Overview

Conventional FODFs were calculated using constrained spherical deconvolution (CSD), as implemented in the MRtrix3 software library (4), from single shell (diffusion weighting b=3000 s/mm^2 applied in 50 directions), whole brain (at 2.5 mm isotropic resolution), 3T MRI data from the BATMAN neuroimaging project hosted by the Open Science Framework [https://osf.io/fkyht/]. The full voxel ('target') FODFs were segmented into constituent fixels by iteratively fitting a cylindrically symmetric, single-fixel FODF model (referred to as F_1) to the target FODF. F_1, shown in fig 1A, was estimated by averaging the rotated FODFs of all voxels used to estimate the white matter signal response function. To maintain cylindrical symmetry, only m=0 spherical harmonic coefficients were kept. The iterative algorithm is described in further detail below.
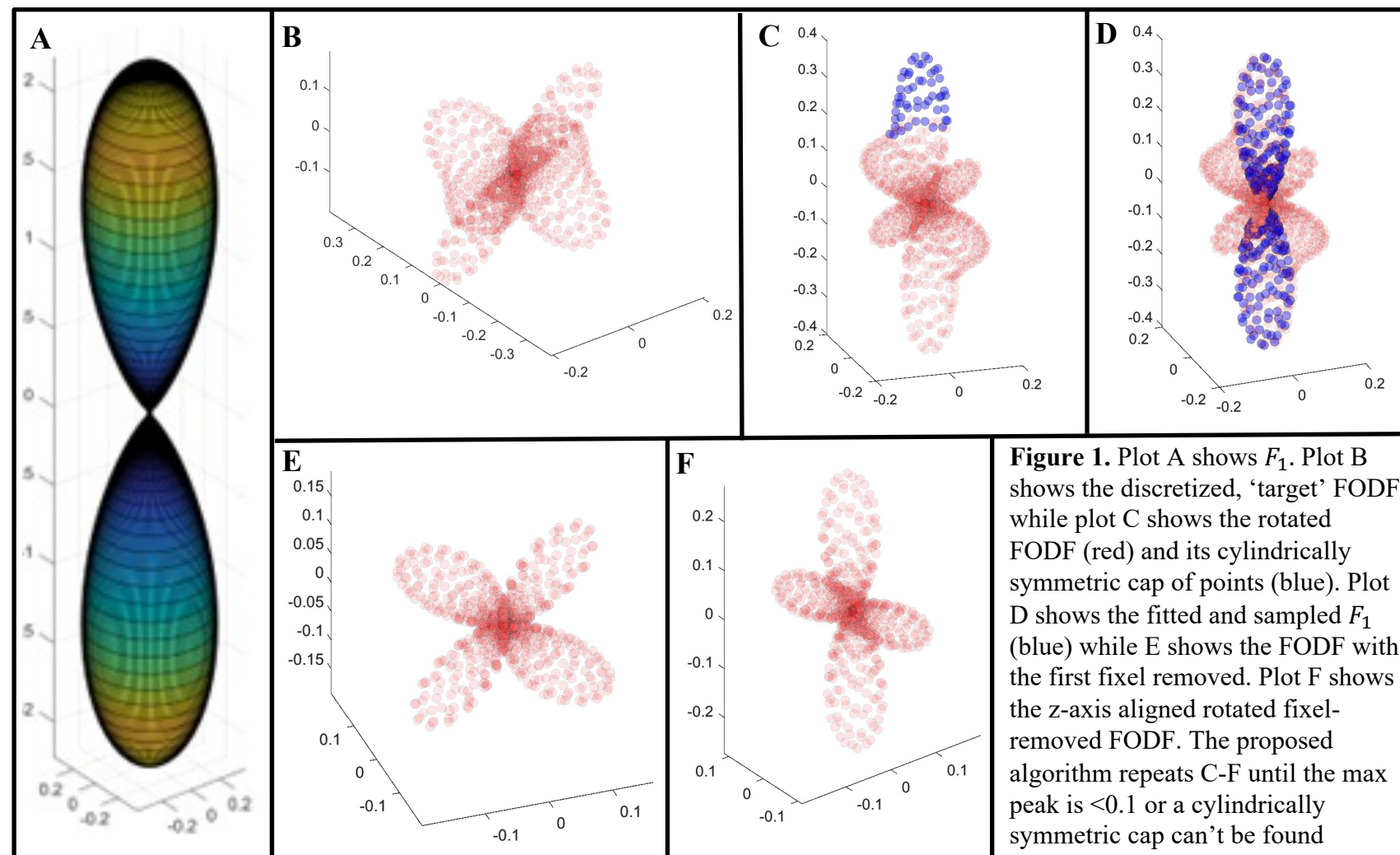

Figure 1. Plot A shows F_1. Plot B shows the discretized, 'target' FODF while plot C shows the rotated FODF (red) and its cylindrically symmetric cap of points (blue). Plot D shows the fitted and sampled F_1 (blue) while E shows the FODF with the first fixel removed. Plot F shows the z-axis aligned rotated fixel-removed FODF. The proposed algorithm repeats C-F until the max peak is <0.1 or a cylindrically symmetric cap can't be found

1. The spherical harmonic representation of the FODF to be analyzed is sampled with equidistant angular resolution. These angles for sampling are derived from tessellated icosahedron. 1922 directions were sampled. (Fig. 1, plot A).
2. The radial peak of the discretized FODF is oriented towards the z axis. A cylindrically symmetric, radius-restricted cap of points centered around this radial peak is identified by comparing the eigenvalues of the second moment of the point coordinates. (Fig. 1, plots B and C).
3. F_1 is rotated and scaled (with LSS) to align with this cap, then subtracted across the entire unit sphere. (Fig .1, plots E and F).

Steps 2 and 3 are repeated until the maximum peak is smaller than a threshold (=0.1, consistent with standard practice (4)), or when there exists no cylindrically symmetric cap of points about the maximum peak.

Cap Selection

The similarity threshold is defined as the relative difference between eigenvalues of the cap's selected points second moment expressed as a percentage. Our most robust algorithm used a stepped threshold selection, wherein, while max radial height is > 0.1, the most restrictive similarity threshold (80%) is first used for cap selection, with the threshold stepping down (by 5%) until a cylindrically symmetric cap with < 3 points is found, or the algorithm steps out of its loop (with no cap of > 50% similarity between eigenvalues able to be found.)

Figure 2, which shows how similarity threshold impacts cap selection, provides support for the use of a stepped threshold. With too restrictive a similarity threshold, two fixels of ~ equal heights at angles of ~25-35 degrees will result in zero fixels found. Our stepping protocol allows first for selection of the most cylindrically symmetric cap, but still allows for our algorithm to find a fixel in these unique cases.
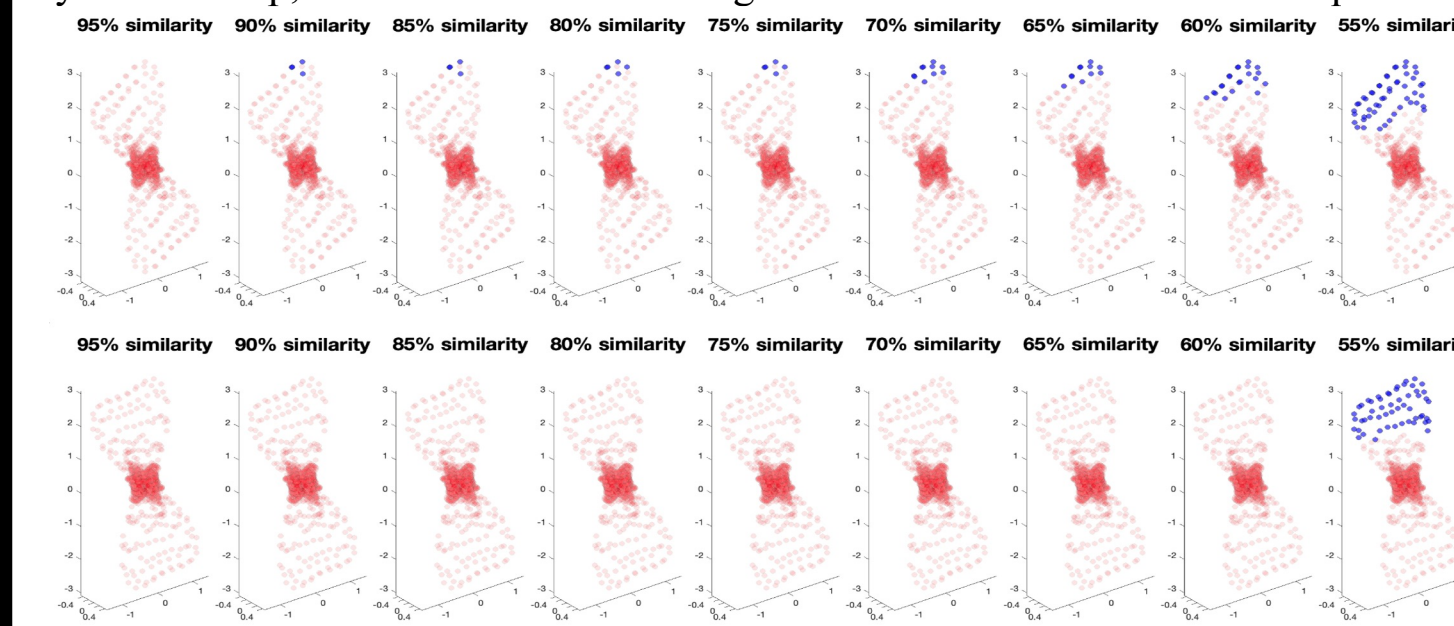

Figure 2. The chosen similarity threshold between eigenvalues has a marked effect on the identified cap. Both rows show the cap selected on a 2-fixel simulated FODF whose fixels are separated by 30 degrees. The top rows' FODF's constituent fixels have a ratio of magnitudes of 1.11:1, while the bottom rows fixels have a ratio of magnitudes of 1:1.

Results

Algorithm performance was evaluated on a full brain dataset. We compared the algorithm's performance to both the 'peak finding' fixel segmentation method (4), and the method proposed in SIFT (6). All three fixel segmentation protocols were identically constrained (minimum fixel height = 0.1). Our algorithm was able to identify 89,140 viable fixels, finding multiple fixels in 48.46% of WM voxels. The geometric continuity filter (at 35 degrees) identified ~4,300 (4.7%) fixels as erroneous. Meanwhile, the best performing lobe-based method, SIFT, could only find 81,806 fixels, with multiple fixels in 41.88% of WM voxels (Fig 4). Improved fixel segmentations are shown in Figure 5. Our algorithm was able to detect fixels less than 40 degrees apart in 18.01% of WM voxels, compared to 1.77% of WM voxels with 'peak finding' and 0.81% of WM voxels with SIFT. Figure 6 illustrates the distribution of minimum interfixel angles in multifixel voxels. With simulated FODFs, our algorithm showed an interfiber angular resolution of ~20-25 degrees (varying with constituent fixel magnitude ratio), which is consistent with the experimental data in Figure 6.

Figure 4. Plot A shows the distribution of the number of fixels per voxel in the white matter resulting from our proposed algorithm. Our algorithm was able to find and validate 89,140 fixels. Further, it identified multiple fixels in 48.5% of white matter voxels. Plots B and C show the distribution of the number of fixels per voxel in the white matter resulting from the SIFT algorithm and peak finding segmentation algorithm, respectively. The SIFT method was able to identify only 81,806 fixels, while the peak finding algorithm found 80,452 fixels. These algorithms were able to identify multiple fixels in 41.6% and 41.9% of WM voxels, respectively. Hence, the new method finds many (9.0% more) fixels that are unresolved by conventional methods.
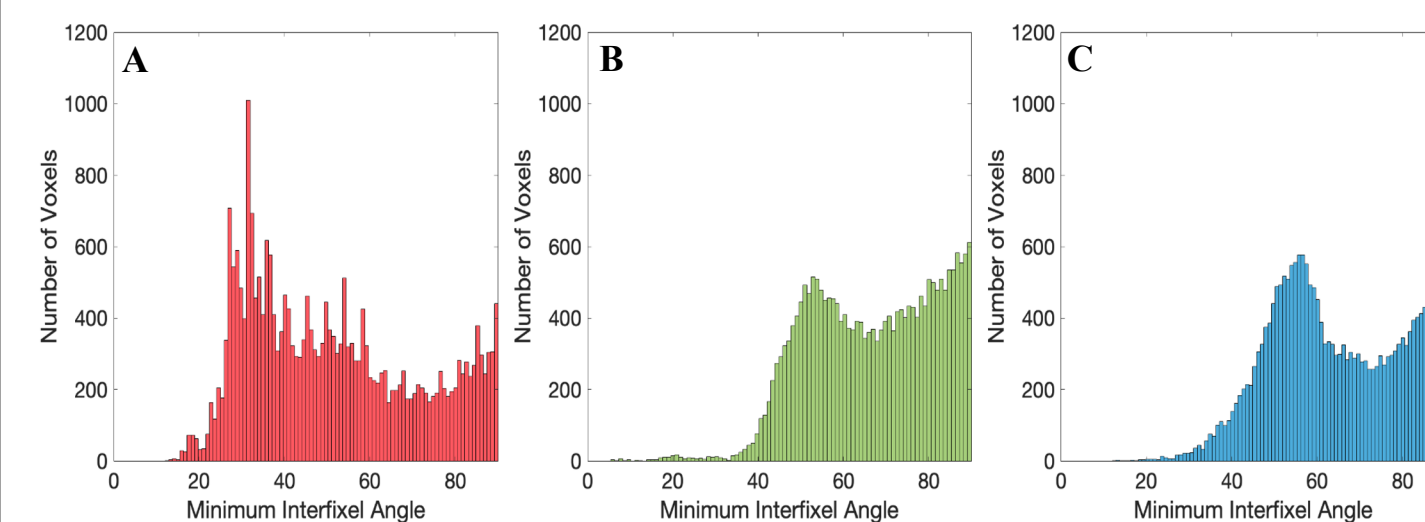

Figure 6: Plot A) shows the distribution of the minimum intefixel angle in multi-fixel voxels when fixels are segmented with our algorithm. Plot B) shows this distribution with results from the SIFT method, and Plot C) shows this distribution with results from the 'peak finding' method. Although our algorithm had a stricter interfixel limit, it was able to resolve appreciably more fixels below the resolution limit of the other methods (about 35-40 degrees of separation).

Figure 5. This plot uses the mrview tool of MRtrix3 to compare the results of our FODF fixel segmentation (B) to the segmentation using the SIFT method (C) in a frontal area (A), known to have many crossing fibers from the corpus callosum and anterior corona radiata.

Model Validation

The fixel models were validated using fiber information from the nearest-neighbor voxels. A voxel's fixel model was considered acceptable when each candidate fixel deviated < 35 degrees from matching fixels in the nearest-neighbor voxels (5). Figure 3 shows an example of this geometric validation.
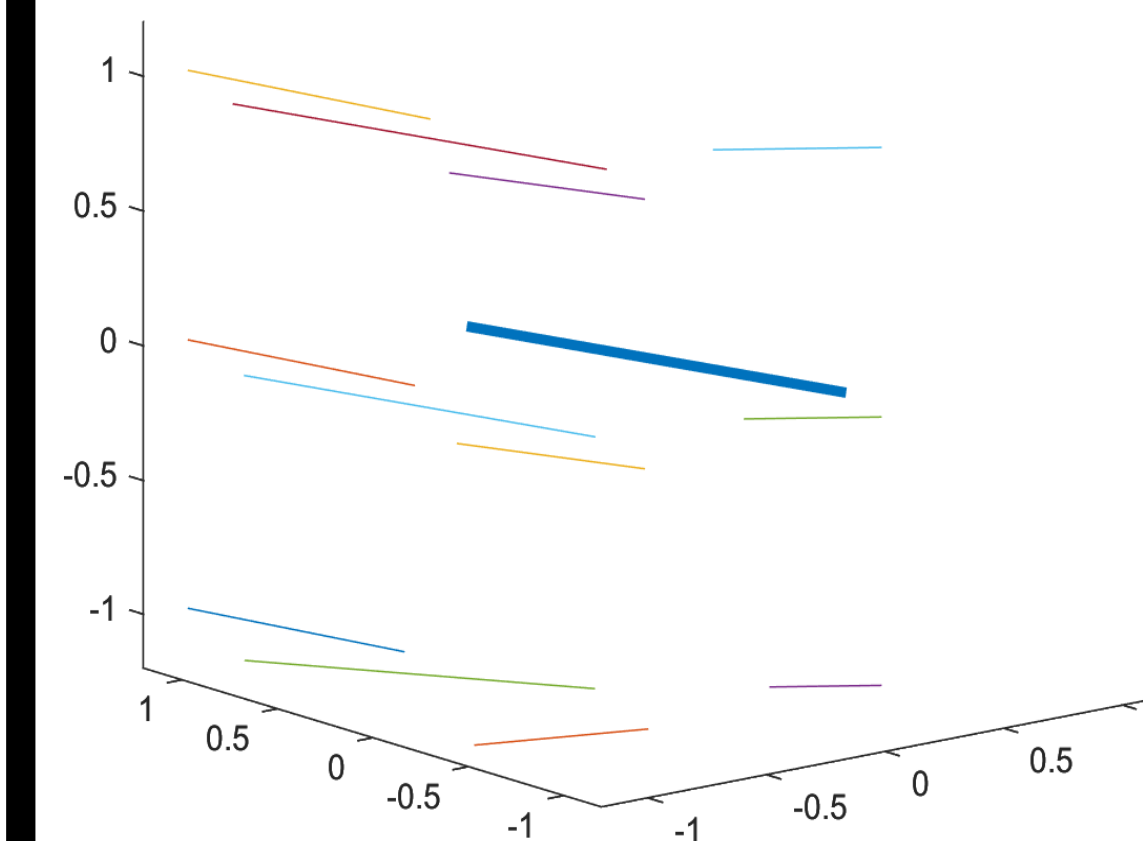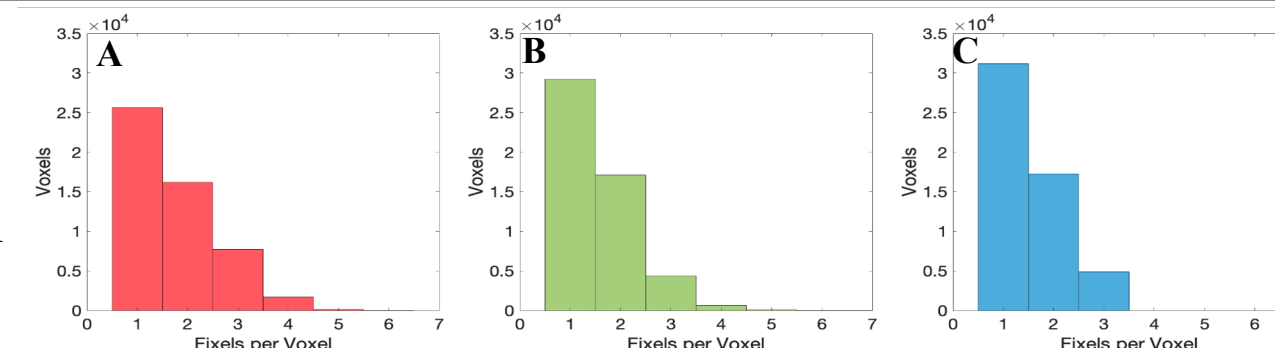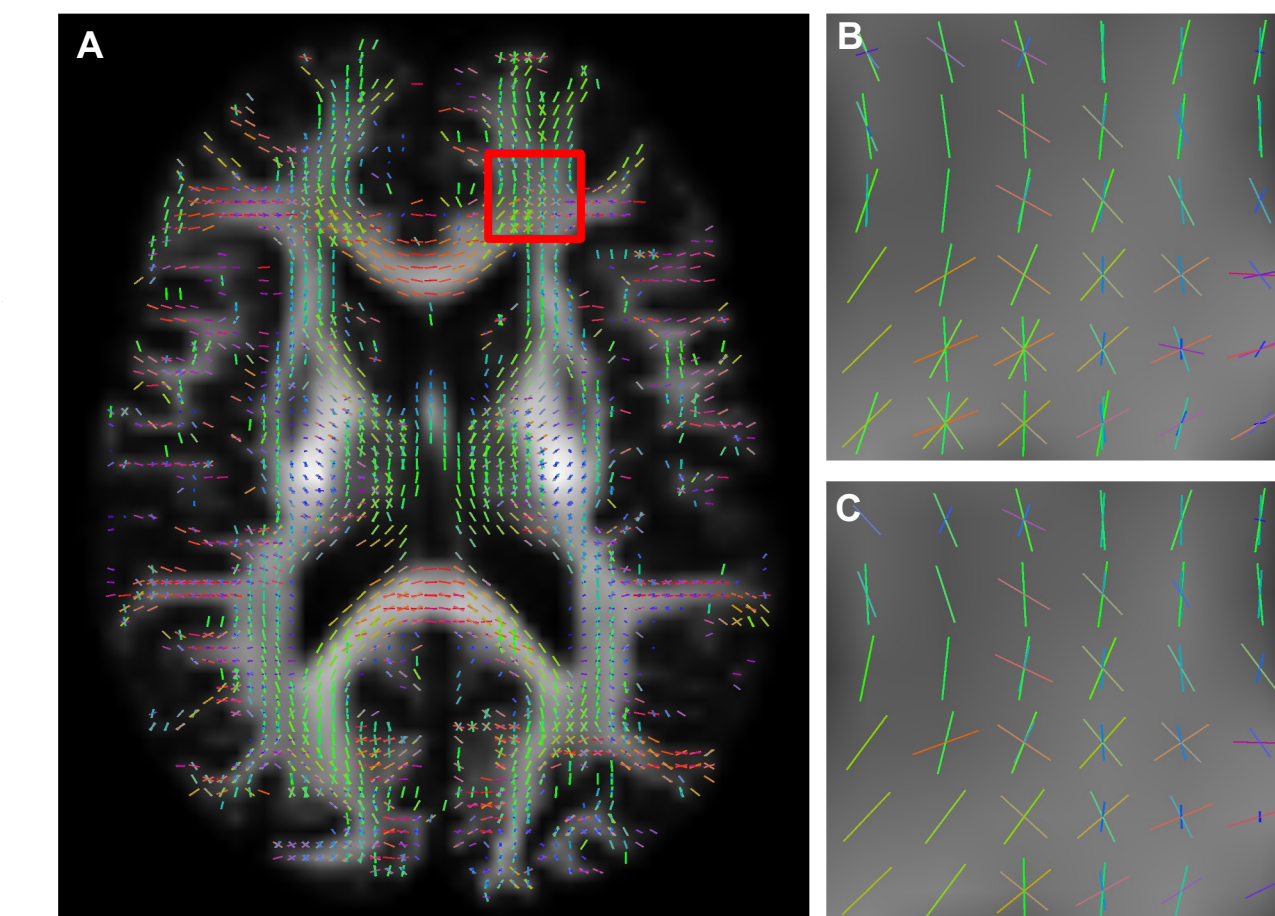

Figure 3. The bold fixel (centered at 0,0,0) is the fixel that is being validated. The thin fixels are those from surrounding voxels which are oriented approximately parallel (< 35°) to the central fixel. These concordant fixels are discrete samples of a curved fiber pathway.

Conclusions

The proposed algorithm offers marked improvements in interfixel angular resolution over conventional lobe based segmentation methods. The new algorithm identifies more fixels per voxel on average and those fixels are supported by concordant fixel geometry in neighboring voxels. This increased angular resolution has the potential to improve the accuracy of fiber tractography and tissue characterization, which in turn may increase reliability of fiber tracking in neurosurgical and other clinical applications.

Future Work

- Develop calculations for apparent fiber density (AFD), dispersion per fixel, and other metrics commonly used in fixel-based analysis (FBA)
- Compare segmented fixels to histological staining.
- Scale single-fixel FODF model with more degrees of freedom (thinning and thickening of the lobes as opposed to just radial scaling.
- Investigate use of geometric continuity filter as a means of FODF noise reduction

Works Cited

1. Jeurissen, Ben, et al. "Investigating the Prevalence of Complex Fiber Configurations in White Matter Tissue with Diffusion Magnetic Resonance Imaging." Human Brain Mapping, vol. 34, no. 11, 2012, pp. 2747–2766., https://doi.org/10.1002/hbm.22099.
2. Anderson, Adam W. "Measurement of Fiber Orientation Distributions Using High Angular Resolution Diffusion Imaging." Magnetic Resonance in Medicine, vol. 54, no. 5, 2005, pp. 1194–1206., https://doi.org/10.1002/mrm.20667.
3. Tuch, David S. "Q-Ball Imaging." Magnetic Resonance in Medicine, vol. 52, no. 6, 2004, pp. 1358–1372., https://doi.org/10.1002/mrm.20279.
4. J.-D. Tournier, R. E. Smith, D. Raffelt, R. Tabbara, T. Dhollander, M. Pietsch, D. Christiaens, B. Jeurissen, C.-H. Yeh, and A. Connelly. MRtrix3: A fast, flexible and open software framework for medical image processing and visualisation. NeuroImage, 202 (2019), pp. 116–37.
5. Schilling, Kurt, et al. "Confirmation of a Gyral Bias in Diffusion MRI Fiber Tractography." Human Brain Mapping, vol. 39, no. 3, 2017, pp. 1449–1466., https://doi.org/10.1002/hbm.23936.
6. Smith, Robert E., et al. "SIFT: Spherical-Deconvolution Informed Filtering of Tractograms." NeuroImage, vol. 67, 2013, pp. 298–312., https://doi.org/10.1016/j.neuroimage.2012.11.049